HYDRODYNAMICS OF THE FREEBOARD REGION OF A FLUIDIZED BED WITH SECONDARY AIR INJECTION

M.Koksal, R.S. Zayed & F. Hamdullahpur

Department of Mechanical Engineering, Dalhousie University, B3J 2X4, Halifax, NS, Canada

ABSTRACT

Gas and particle flow dynamics in the freeboard region of a bubbling fluidized bed was investigated. The results of the swirling lateral air injection measurements showed that the presence of swirl increased the solid internal circulation and residence time. In the experiments without the secondary air injection, the particles were accelerated in the axial direction reaching a maximum velocity at a certain height in the freeboard due to high drag forces exerted on the particles by the gas puffs emerging from bubbles coalescing near the bed surface. The theoretical part of this study involves a 2-D Eulerian-Eulerian (two-fluid) approach using kinetic theory of granular solids to model the bubbling dense region and the freeboard together.

INTRODUCTION

Atmospheric pressure bubbling fluidized beds are viable options to costly circulating systems in small capacity power generation and retrofit applications. Furthermore, they are broadly used in other physical or chemical processing applications, such as drying, coating, catalytic cracking and gasification. The design procedure for a bubbling bed reactor, be it a reacting or non-reacting type, involves the design of two very closely interrelated regions; the dense bed and the freeboard. The freeboard region provides physical space for additional and complimentary gas-gas and gas-solid reactions/contacting to take place under a completely different hydrodynamic behavior than that of the dense bed.

The bubble-induced turbulent gas flow field in the freeboard is the predominant effect on the motion of particles. Knowledge of particle and gas motion in the freeboard is essential for improving the performance of the bubbling fluidized beds. For example, previous studies indicate that due to the bubbling nature of fluidized bed combustors (FBC), gas-gas mixing is limited by the action of large scale eddies in the form of isolated gas pockets [1,2].

Injection of secondary air into the freeboard of FBC units can be used to introduce a tangential component to the velocity vector of the upward-moving plug flow like field, thus, creating a shear flow between the isolated air pockets and the surrounding air flow. It also creates a cyclonic air motion. The net result is increased turbulence, increased solid residence time, and a reduction in NOx emissions due to reaction of NO and char particles [3,4].

Several studies on modeling the particle motion in the freeboard of bubbling fluidized beds are available in the literature [5,6,7,8]. These studies are all based on solving the equation of motion of a particle to predict the particle trajectory in a laminar gas flow field with a predetermined particle ejection velocity at the bed surface. However, the studies of Horio et al. [9] and Hamdullahpur and MacKay, [2] showed high levels of velocity fluctuations in the freeboard caused by the erupting bubbles near the bed surface indicating the significance of particle-turbulence interaction. Also, there is not a general consensus on the value of the particle ejection velocity, as physically the origin of the ejected particles remains unclear.

The first stage of the theoretical approach in this study involves a 2-D Eulerian-Eulerian (two-fluid) approach to simulate the bubbling dense region and the freeboard together taking the gas phase turbulence into account. This is one of the promising and developing methods in modeling of gas-solid systems especially with high solid loading, such as fluidized beds [10,11,12,13]. In this approach, the solid phase is also handled as a continuum like the gas phase. The gas and solid phases are described by similar mass and momentum balances. These balances are coupled by an interphase drag force. The solid phase closures are obtained from the kinetic theory of granular solids [14,15].

EXPERIMENTAL

A cold fluidized bed system was designed and built to allow for the measurement of particle motion in the freeboard region under swirling lateral air injection conditions (Fig.1). The bed was constructed from modular cylindrical plexiglass sections (0.3 m diameter and 0.0064 m wall thickness) so that the tangential inlet ports could be located at different elevations above the bed and visual observation of the flow was allowed. The plastic sections were electrically grounded to minimize interference by triboelectric charging. A section 300 mm high was however constructed of first quality Crown Glass to insure good optical access for the LDA beams. The total height of the column is 1. 35 m. At the top of the column a vortex finder (0.15 m in diameter and 0.19 m long) was mounted and connected to a cyclone to recover the elutriated solids.

Sand particles (d_p=110μm, ρ_p=2600 kg/m^3, U_t=0.78 m/s) were fluidized with ambient air. The static bed height was 0.15 m. The superficial gas velocity was adjusted using a variable speed blower and monitored by a calibrated orifice meter. A perforated aluminum plate, placed on the top of a 200 mm packed section, was used to distribute the air uniformly across the bed. The distributor plate was 5 mm thick through which 295 holes (2.05 mm in diameter) were drilled in a square pattern (15 mm pitch) to yield 1.5 % open area fraction.

The freeboard swirl generator was designed using principles of those cyclone dust separators. It has four identical ports (placed 90° apart) for a total inlet tangential area of 116 cm^2. In this study, the swirl generator was placed 95 cm above the static bed in the freeboard region. The swirl number (SN) which is defined as the axial flux of swirl or angular momentum divided by the axial flux of the axial momentum was varied 0 to 0.8 by adjusting the ratio of the secondary air to primary air flow rates.

Particle velocity was measured using laser Doppler anemometer. A 2 watt Argon-Ion laser was used to drive a two-channel on-axis LDA (TSI Model 9100). The LDA was operated in the backscatter model to facilitate the axial and radial traversing of the freeboard. An IBM PC compatible microcomputer was used for data storage and off-line processing of time series. A Bragg cell was used for simultaneous measurement of ascending and descending particle velocities. Criteria were established for settings of frequency shift, elocctronic filters, gain and other electronic settings as a function of local flow conditions and were applied to obtain a low noise to signal ratio [16]. Particle axial, radial and tangential velocities were measured at different locations in the freeboard for superficial gas velocities of 18, 25, 35 cm/s at heights 13 to 40 cm above the static bed.

THEORETICAL

The reader is referred to studies of Gidaspow and Enwald et al. for in-depth explanation of Eulerian approach applied to fluidization [10,17]. The following equations in Cartesian tensor notation are obtained by ensemble averaging the local instantaneous equations and jump conditions. Assuming no chemical reaction and isothermal condition, the following equations are written for the gas and the solid phase mass balances;

$$\frac{\partial(\varepsilon\rho)_g}{\partial t}+\frac{\partial(\varepsilon\rho U_i)_g}{\partial x_i}=0 \quad [1]$$

$$\frac{\partial(\varepsilon\rho)_s}{\partial t}+\frac{\partial(\varepsilon\rho U_i)_s}{\partial x_i}=0 \quad [2]$$

The gas phase momentum balance can be expressed as;

$$\frac{\partial(\varepsilon\rho U_j)_g}{\partial t}+\frac{\partial(\varepsilon\rho U_i U_j)_g}{\partial x_i}=-\varepsilon_g\frac{\partial P}{\partial x_j}+\frac{\partial(\varepsilon_g\tau_{ij,l})}{\partial x_i}+\frac{\partial(\varepsilon_g\tau_{ij,t})}{\partial x_i}+\varepsilon_g\rho_g g_j+K_{fs,j}(U_{j,s}-U_{j,g}) \quad [3]$$

The gas laminar stress tensor can be written as;

$$\tau_{ij,l}=\mu_l\left[\left(\frac{\partial U_j}{\partial x_i}+\frac{\partial U_i}{\partial x_j}\right)-\frac{2}{3}\delta_{ij}\frac{\partial U_k}{\partial x_k}\right] \quad [4]$$

The gas phase turbulent stress tensor following Boussinesq is;

$$\tau_{ij,t}=\mu_t\left[\left(\frac{\partial U_j}{\partial x_i}+\frac{\partial U_i}{\partial x_j}\right)-\frac{2}{3}\delta_{ij}\frac{\partial U_k}{\partial x_k}\right]-\rho\frac{2}{3}k\delta_{ij} \quad [5]$$

The solid phase momentum balance can be written as;

$$\frac{\partial(\varepsilon\rho U_j)_s}{\partial t}+\frac{\partial(\varepsilon\rho U_i U_j)_s}{\partial x_i}=-\varepsilon_s\frac{\partial P}{\partial x_j}+\frac{\partial(\varepsilon_s\tau_{ij,s})}{\partial x_i}+\varepsilon_s\rho_s g_j+K_{fs,j}(U_{j,g}-U_j) \quad [6]$$

The solid phase stress tensor is

$$\tau_{ij,s}=\mu_s\left[\left(\frac{\partial U_j}{\partial x_i}+\frac{\partial U_i}{\partial x_j}\right)-\frac{2}{3}\delta_{ij}\frac{\partial U_k}{\partial x_k}\right]-P_s\delta_{ij}+\xi_s\delta_{ij}\frac{\partial U_k}{\partial x_k} \quad [7]$$

The fluid-solid exchange coefficient, K_{fs}, has a form derived by Sylamlal at al. [18].

$$K_{fs}=\frac{3\varepsilon_s\varepsilon_g\rho_g}{4v_t^2 d_p}C_D\left(\frac{Re_p}{v_t}\right)\left|\vec{U}_s-\vec{U}_g\right| \quad [8]$$

$$Re_p=\frac{\rho_g d_p\left|\vec{U}_s-\vec{U}_g\right|}{\mu_g}$$

$$v_t=0.5\left(A-0.06Re_p+\sqrt{(0.06Re_p)^2+0.12Re_p(2B-A)+A^2}\right)$$

$$A=\varepsilon_g^{4.14} \quad \text{and} \quad B=0.8\varepsilon_g^{1.28} \text{ for } \varepsilon_s\le 0.85$$

and $B=\varepsilon_g^{2.65}$ for $\varepsilon_s > 0.85$ and $C_D=\left(0.63+\frac{4.8}{\sqrt{Re_p/v_t}}\right)^2$

The solid phase pressure is suggested by Jenkins and Savage, and Ding and Gidaspow, [14, 11]:

$$P_s=\varepsilon_s\rho_s\theta_s+2\rho_s(1+e)\varepsilon_s^2 g_o\theta_s \quad [9]$$

θ_s is the so-called granular temperature, which describes the fluctuation kinetic energy of the particles. It is defined as;

$$\frac{3}{2}\theta_s=\frac{1}{2}\overline{C_s^2} \quad [10]$$

The radial distribution function used in this study has the following form [18]:

$$g_o=\frac{1}{1-\varepsilon_s}+\frac{3\varepsilon_s}{2(1-\varepsilon_s)^2} \quad [11]$$

Solid phase bulk viscosity [11, 18,19]:

$$\xi_s=\frac{4}{3}\varepsilon_s^2\rho_s d_p g_o(1+e)\sqrt{\frac{\theta_s}{\pi}} \quad [12]$$

Solid phase shear viscosity:
The collisional part of the solid phase shear viscosity is suggested by Ding and Gidaspow, Sylamlal et al., and Balzer and Simonin [11,18,19]

$$\mu_{s,coll}=\frac{4}{5}\varepsilon_s\rho_s d_p g_o(1+e)\sqrt{\frac{\theta_s}{\pi}} \quad [13]$$

The kinetic contribution is modeled according to Sylamlal et al. [18]

$$\mu_{s,kin}=\frac{\varepsilon_s d_p\rho_s\sqrt{\theta_s\pi}}{6(3-e)}\left[1+\frac{2}{5}(1+e)(3e-1)\varepsilon_s g_o\right] \quad [14]$$

Solids fluctuating (pseudo-thermal) energy balance [11,18,19]

$$\frac{3}{2}\left[\frac{\partial}{\partial t}(\varepsilon\rho\theta)_s+\frac{\partial(\varepsilon\rho U_i\theta)_s}{\partial x_i}\right]=\tau_{ij,s}\frac{\partial U_{j,s}}{\partial x_i}-\frac{\partial}{\partial x_i}\left[k_{\theta s}\frac{\partial\theta_s}{\partial x_i}\right]-\gamma_{\theta s}+\phi_{fs} \quad [15]$$

Following Lun et al. [15];

$$\gamma_{\theta_s}=\frac{12(1-e^2)g_o}{d_p\sqrt{\pi}}\rho_s\varepsilon_s^2\theta_s^{3/2} \quad [16]$$

and Sylamlal et al. [18]

$$k_{\theta s}=\frac{15d_p\rho_s\varepsilon_s\sqrt{\theta\pi}}{4(41-33\eta)}\left[1+\frac{12}{5}\eta^2(4\eta-3)\varepsilon_s g_o+\frac{16}{15\pi}(41-33\eta)\eta\varepsilon_s g_o)\right]$$

in which $\eta=0.5(1+e)$ and from Gidaspow et al. [21]

$$\phi_{fs}=-3K_{fs}\theta_s \quad [18]$$

SIMULATIONS

The grid generation and the simulations were carried out by Fluent V4.4. The computational domain illustrated in Figure 2 is made up of uniform Cartesian grid of 41×41. The gas density and viscosity were 1.21 kg/m^3 and 1.79E-05 kg/m.s. Two different coefficient of restitution values were used; 0.6 and 0.8. Due to highly transient behavior of the problem, the time step used in the simulations was chosen as 0.0005 s, which makes the average convective Courant number to be 0.012. Initially, the first 15cm (static bed height) of the domain is set to be closely packed with sand particles with a volume fraction of 0.59. A uniform superficial gas velocity is fed from the bottom at a rate of 35cm/s. At the outlet of the domain, “outlet boundary” condition (all the fluxes vanish) is applied. The turbulent intensity of the gas is chosen to be 5 % at inlet. Fluent V4.4 uses zero flux for the granular temperature at the solid boundaries. “No slip” condition is used for the gas and the solid phase.

A control volume based technique is employed to solve the conservation equations described for the model. In this technique, the domain is divided into discrete control volumes using a general curvilinear grid and the governing equations are

integrated on the individual control volumes to construct the algebraic equations for discrete unknowns to be solved. The LGS (Line Gauss Seidel) method is used to solve the algebraic equations. For evaluation of the convective transport terms the power law scheme is used.

RESULTS AND DISCUSSION

Figure 3 shows the variation of the descending and ascending axial particle velocity with the bed height on the centerline of the bed without secondary air injection (SN=0.0) for superficial gas velocities of 25 and 35 cm/s. In the absence of swirl, the average particle velocity increases to a maximum before starting to decay in the freeboard. This behavior may be explained on the basis that the gas emerges at the bed surface in the forms of "gas puffs" with higher velocity than the surrounding gas. These gas puffs are formed as a result of bubble coalescence. During their rise in the freeboard, the puffs exert a high drag force on the particles resulting in the acceleration of the particles until the puffs dissipate their momentum and disperse into the bulk flow, or the particle separates from them. After that, the particles start to decelerate in the freeboard.

Figure 4 shows the radial distribution of the particle tangential velocities at different swirl numbers. Due to the injection of secondary swirling air into the freeboard, the particles gain a strong tangential velocity component as seen in Fig. 4. Figure 4 also shows that the particles have small negative tangential velocities at the column center. This maybe due to the existence of a weak reverse gas flow zone at the column center similar to that observed in cyclone flow. The tangential velocity component is found to increase with increasing swirl numbers at all elevations and fluidization velocities.

The measured mean particle axial velocity for different swirl numbers is shown in Figure 5. The results obtained, for SN=0.0, indicate that at any particular location or fluidization velocity, the mean particle axial velocity does not necessarily have to be close to zero as suggested by Levy and Lockwood [20]. This is particularly true when the swirl is applied in the freeboard area where definite circulation patterns are formed as a result of the imposition of swirl. This pattern can be clearly seen at an elevation of 21 cm above the static bed height. The application of swirl is generally found to increase the mean particle velocity in the central region of the column and to create a net downward moving region near the wall.

The effect of swirl number on the experimentally determined mean particle radial velocity can be seen on Figure 6. The particles gain a strong radial velocity component due to the influence of the centrifugal force created by the swirl. This effect increases with increasing swirl number. At SN=0.0, it is interesting to note that the mean velocity by which the particles are injected into the freeboard has a slight radial velocity component which reaches a peak near the wall and then decreases or dampens in the near vicinity of the wall. This indicates a slight solid circulation pattern in which solid particles are ejected at the bed surface into the direction of the walls where they fall downward.

Figure 7 shows the simulated instantaneous void fraction contours and the sand velocity vectors for U_0=35 cm/s. As can be inferred from the figure, the two-fluid model captures the basic hydrodynamic essentials of the dense bed qualitatively. Bubbles form at the bottom of the bed, their shape are influenced by the neighboring bubbles and bubble coalescence are observed. The solid circulation around the bubbles as they rise up and the bursting of the bubbles at the bed surface are well predicted. The acceleration of the solid particles in the wake of the bubble as the bubble collapses at the bed surface in Figure 7 is worth noting as this is one of the particle ejection mechanisms into the freeboard.

Figure 8 presents the simulated mean axial velocity of the ascending particles for U_0=35 cm/s averaged for 3 s at the centerline of the bed. It is interesting to note that the tendency of the increase in the average particle axial velocity to a maximum and than its decay is predicted as measured in the experiments. The maximum velocity is predicted as 60 cm/s whereas it is measured 35 cm/s in the experiments. The main discrepancy between the experiments and the simulations is the height at which the axial velocity decays. In the simulations, the particles could reach to a distance 20 cm above the bed surface whereas in the experiments ascending particle velocities were measured at 40 cm above the bed surface. The reason may be due to the drag function used or the modeling of the turbulence particle interaction. The effect of the bubble induced turbulence on the particles were addressed in the studies of Horio et al. [9] and Hamdullahpur et al. [2]. As can be seen from Figure 8, using a turbulence model (a modified two-equation (k-ε) model that takes the effect of the particle phase on the gas phase turbulence) in the gas phase significantly improves the predictions when compared to the case with a laminar gas flow. But, still the form of the kinetic theory used in this study does not consider the effect of interstitial gas on the particle phase shear and bulk viscosities (Equations 12, 13, 14). This is the main reason why this description of kinetic theory may break up in the dilute regions where the particle velocity fluctuations and dispersion are determined by the fluid turbulence rather than the particle-particle collisions. A more general description of including the effect of the interstitial gas can be found in Balzer et al. [13].

Figure 9 shows the effect of the coefficient of restitution on the mean axial velocity in the radial direction for U_0=35 cm/s. The coefficient of restitution describes the loss of kinetic energy during a collision. The value of the coefficient of restitution effects the results significantly especially in dense suspensions while its influence is small in dilute regions [13]. As can be inferred from Figure 9, the magnitude of the mean axial velocity for the case with e=0.6 is larger than the magnitude of the mean axial velocity case with e=0.8 for the same superficial gas velocity, indicating the increase of the height of the splash zone. This direct effect of the dense phase region on the freeboard region is due to the increase in the bubble size with decreasing coefficient of restitution. Because, for dense suspensions, a decrease of the coefficient of restitution causes the granular temperature to decrease. This in turn causes a decrease in the viscosity and diffusion resulting in larger gradients and more bubble in the calculated results. The bursting of the bigger bubbles at the bed surface creates more agitation in the freeboard, ejecting the particles with a larger velocity to a higher distance in the freeboard.

The next stage to model the freeboard region involves 3-D modeling of the upward moving gas-solid flow and the secondary air flow. This part of the work is still in progress.

NOMENCLATURE

C_D	drag coefficient
C_s	fluctuating particle velocity
d_p	particle diameter, m
e	coefficient of restitution
g_j	j-direction of gravity
g_o	radial distribution function
k_θ	diffusion coefficient for pseudo-thermal energy
K_{fs}	fluid-solid momentum exchange coefficient
P	pressure, Pa
Re	Reynolds number
t	time, s
U_i, U_j	i and j Components of Velocity Vectors
Z	height above the static bed height, cm

Greek Letters

ε	volume fraction
γ	collisional energy dissipation
δ_{ij}	Kronecker Delta
θ	granular temperature, m^2/s^2
ξ	solids bulk viscosity
μ	shear viscosity, Pa.sec
ϕ_{fs}	energy exchange between the fluid and the solids.
ρ	density, kg/m^3
τ	stress tensor

Subscripts

g gas phase
s particle phase
l laminar
t turbulent

REFERENCES

1. Pemberton, S.T., Davidson, J.F., "Turbulence in the Freeboard of a Gas Fluidized Bed", Chemical Engineering Science, vol. 39, No. 5, pp. 829-835, 1984.
2. Hamdullahpur, F., MacKay, G.D.M., "Two-Phase Behaviour in the Freeboard of a Gas Fluidized Bed", AIChE Journal, vol. 32, no. 12, pp. 2047-2055, 1986.
3. Nieh, S., Yang, G., "Particle Flow Pattern in the Freeboard of a Vortexing Fluidized Bed", Powder Technology, vol. 50, no. 1, 1987.
4. Hamdullahpur, F., Zayed, R.S., Khawaja, E.El., "NO_x reduction in Fluidized Bed Combustors", Proceedings of the American Flame Research Committee's 1989 International Symposium on Combustion in Industrial Furnaces and Boilers, New Jersey, pp. 5.1-5.10, 1989.
5. Zenz, F.A., Weil, N.A., "A Theoretical-Emprical Model to the Mechanism of Particle Entrainment from Fluidized Bed", AIChE J, vol. 4., 1958.
6. Do, H.T., Grace, J.R., Clift, R., "Particle Ejection and Entrainment from Fluidized Bed", Powder Technology, vol. 6, pp. 195, 1972.
7. George, E. E., Grace, J. R., "Entrainment of Particles from Aggregative Fluidized Bed", AIChE Symposium Series, vol. 74, pp. 176, 1978.
8. Berkelmann, K.G., Renz, U., "The Fluid Dynamics in the Freeboard of an FBC-The Use of LDV to Determine Particle Velocity and Size", Proceedings of Fluidization VI, pp. 105-112, Banff, Alberta, 1989.
9. Horio, M., Al. Taki, Y.S. Hsieh, Muchi, I., "Elutriation and Particle Transport Through the Freeboard of a Gas-Solid Fluidized Bed", 3rd International Conference on Fluidization, J.R. Grace and J.M. Matsen, eds., Plenum, New York, 1980.
10. Gidaspow, D., *Multiphase Flow and Fluidization*, Academic Press, 1994.
11. Ding, J., Gidaspow, D., "A Bubbling Fluidization Model Using Kinetic Theory of Granular Flow", AIChE J, vol. 36, no. 4, pp. 523-538, 1990.
12. Boemer, A., Qi, H., Renz, U., "Eulerian Simulation of Bubble Formation at a Jet In a Two-Dimensional Fluidized Bed", Int. J. Multiphase Flow, vol. 23, no. 5, p. 927-944, 1997.
13. Balzer, G., Boelle, A., Simonin, O., "Eulerian Gas-Solid Flow Modeling of Dense Fluidized Bed", Preprints of Fluidization VII, vol. 2, pp. 1125-1134, Tours, France, 1995.
14. Jenkins,J.T., Savage, S.B., "A Theory for Rapid Flow of Identical, Smooth, Nearly Elastic Spherical Particles", J.Fluid Mechanics, vol. 130, pp. 187, 1983.
15. Lun, C.K.K., Savage, S.B., Jeffrey, D.J., Chepurniy, N.,"Kinetic Theories for Granular Flow:Inelastic Particles in Couette Flow and Slightly Inelastic Particles in a General Flow-Field",J.Fluid Mechanics, vol. 140, pp. 223-256, 1984.
16. Zayed, R. S., PhD Dissertation, Technical University of Nova Scotia, 1990.
17. Enwald, H., Peirano, E., Almstedt, A.E., "Eulerian Two-Phase Flow Theory Applied to Fluidization", Int. J. Multiphase Flow, vol. 22, Suppl., pp. 21-66, 1996.
18. Syamlal, M., Rogers, W., O'Brian, T.J., "MFIX Documentation, Theory Guide", technical note DOE/METC-94/10004, 1993.
19. Balzer, G., Simonin, O., "Extension of Eulerian Gas-Solid Flow Modelling to Dense Fluidized Bed", EDF, Report HE-44/93.13, 1993.
20. Levy, Y. , Lockwood, F.C., "Laser Doppler Measurements of Flow in Freeboard of a Fluidized BedBed", AIChE J, vol. 29, pp. 889-895, 1983.
21. Gidaspow, D., Bezbaruah, R., B., Ding, J., "Hydrodynamics of Circulating Fluidized Beds:Kinetic Theory Approach", eds., Potter, O.E., Nicklin, D.J., Fluidization VII, Engineering Foundation, p. 75-82, 1992.

FIGURES

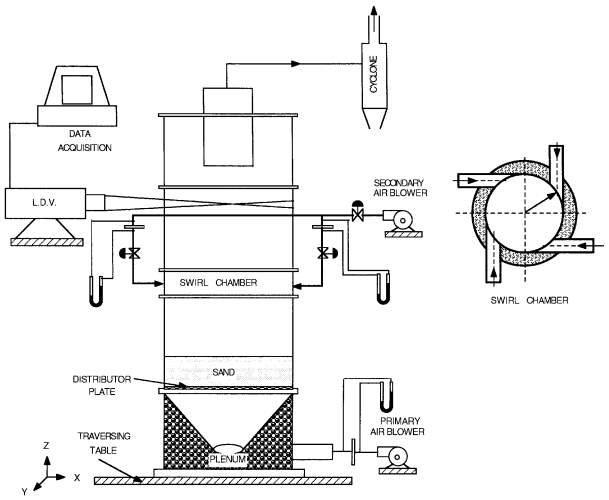

Figure 1. Experimental Setup and the Swirl Chamber

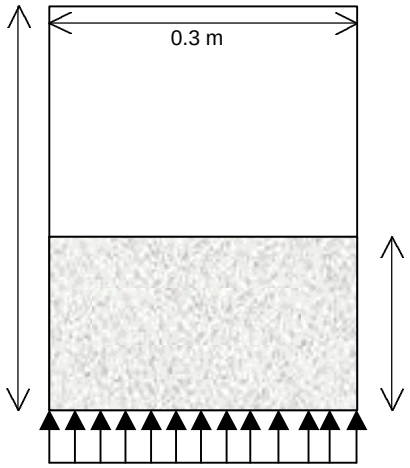

Figure 2. Computational Domain

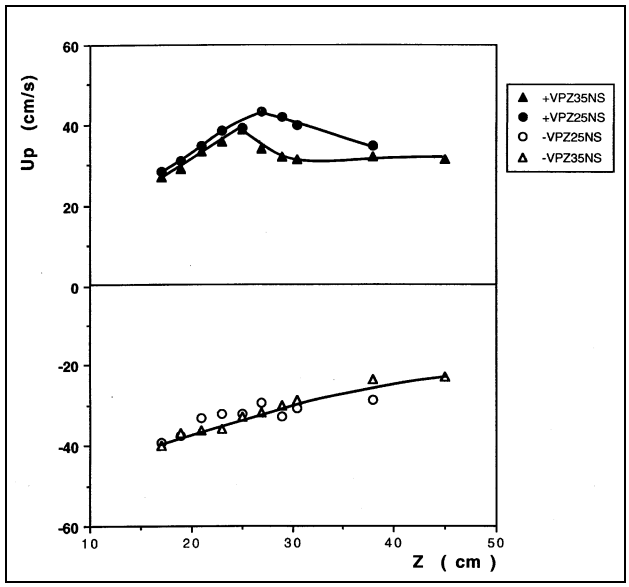

Figure 3. The effect of superficial gas velocity on the particle axial velocity at the center of the column, SN=0.0

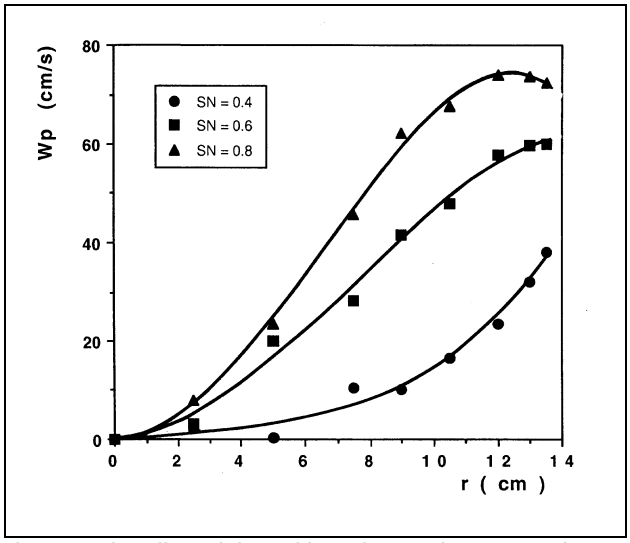

Figure 4. The effect of the swirl number on the measured mean particle tangential velocity in the radial direction, U_o=25 cm/s, Z=21 cm.

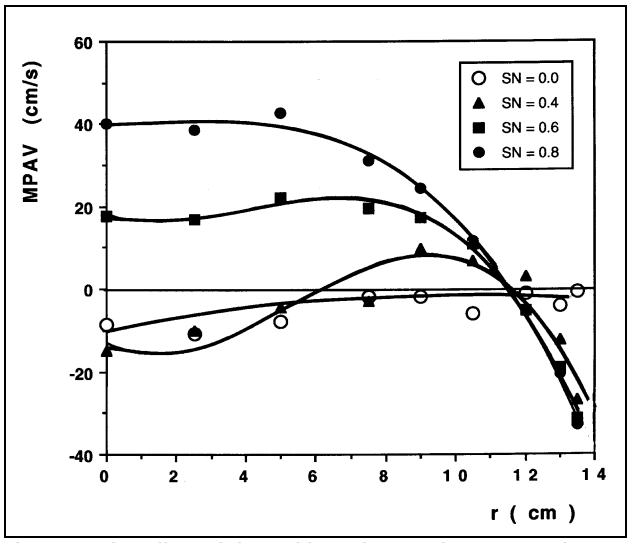

Figure 5. The effect of the swirl number on the measured mean particle axial velocity in the radial direction, U_o=25 cm/s, Z=21 cm.

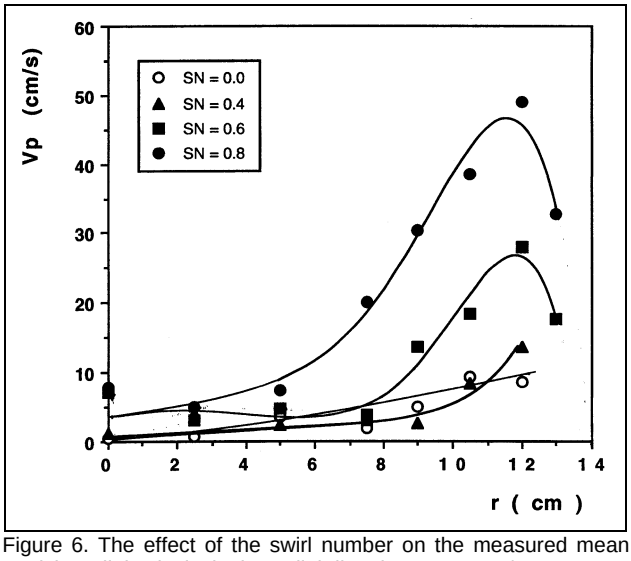

Figure 6. The effect of the swirl number on the measured mean particle radial velocity in the radial direction,U_o=25 cm/s, Z=21 cm.

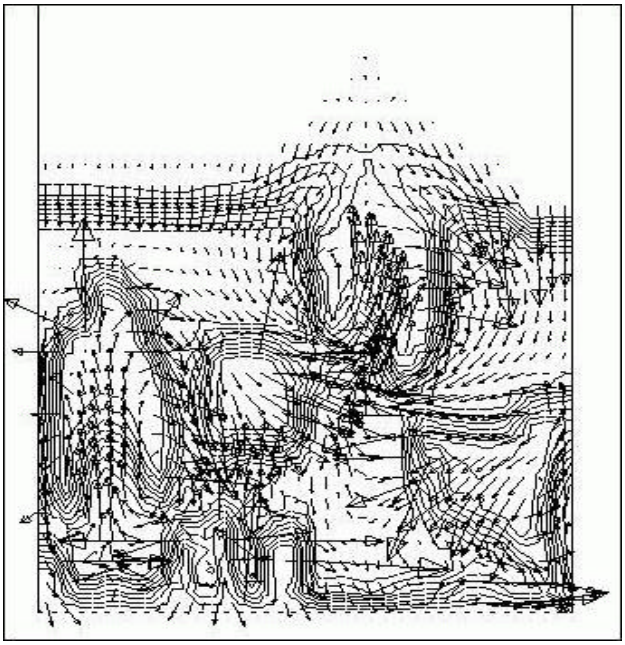

Figure 7. Instantaneous void faction contours and sand velocity vectors, U_o=35 cm/s, e=0.8.

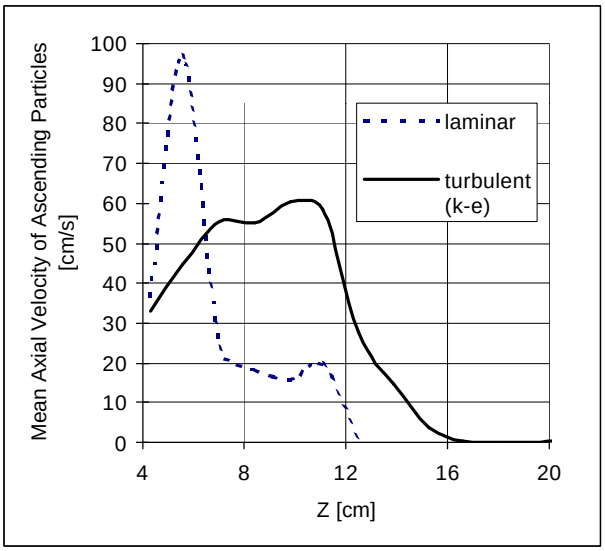

Figure 8. Mean axial velocity of the ascending particles, U_o=35 cm.s, e=0.8.

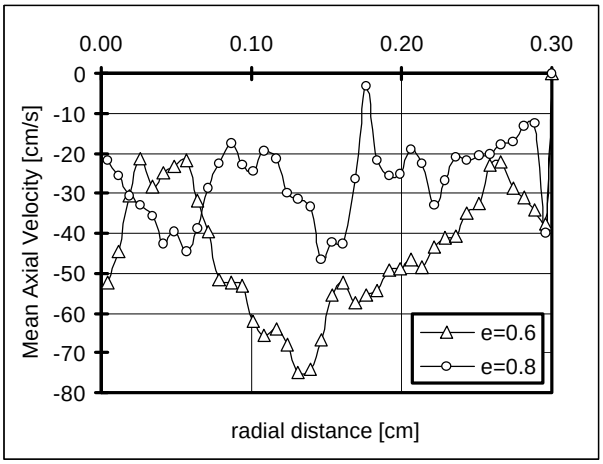

Figure 9. The effect of the coefficient of restitution on the time averaged mean particle velocity in the radial direction, U_o=35 cm/s, Z=15 cm.